Analytical and Bioanalytical Chemistry (2021) 413:1441–1452
https://doi.org/10.1007/s00216-020-03108-3

RESEARCH PAPER

Developing an integrated microfluidic and miniaturized electrochemical biosensor for point of care determination of glucose in human plasma samples

Shamim Azimi[1] · Ali Farahani[2] · Aristides Docoslis[1] · Sahar Vahdatifar[3]

Received: 10 October 2020 / Revised: 22 November 2020 / Accepted: 1 December 2020 / Published online: 2 January 2021

Abstract

A cost-effective, point of care (POC) device based on highly oriented CNT arrays was developed as an electrochemical assay for real-time and sensitive detection of glucose in complex samples. A low-cost, microcontroller-based potentiostat consisting of Arduino Due and LMP9100-EVM was developed to perform electrochemical measurements such as cyclic voltammetry (CV) and amperometry. A syringe pump based on open-source electronics was designed to direct the flow through a microfluidic chip. Vertically aligned carbon nanotube (VACNT) sensor arrays, in combination with the miniature potentiostat and the syringe pumps, were utilized as a POC device for the rapid and accurate detection of glucose. The structure and morphology of samples were characterized by field emission scanning electron microscopy (FESEM) and attenuated total reflectance Fourier transform infrared spectrometry (ATR-FTIR). CV as well as electrochemical impedance spectroscopy (EIS) was performed to investigate the electrochemical behavior of the electrode with respect to different diffusion regimes. The mediator-less biosensor had a limit of detection of 23 μM and sensitivity of 1462 μA mM^{-1} cm^{-2} and 1050 μA mM^{-1} cm^{-2} at the linear range of 1.2–7.8 mM and 7.8–11.2 mM, respectively. The presence of other biological compounds such as uric acid (UA) and ascorbic acid (AA) did not interfere with the detection of glucose. Finally, the designed POC device was successfully applied for the determination of glucose in human blood plasma samples.

Keywords Point of care · VACNTs · Microfluidic device · Electrochemical biosensor · Cyclic voltammetry

Introduction

Glucose, as the major source of energy for cells, is transported to cells through insulin in the bloodstream. The human body adjusts blood glucose levels at the concentration range of 4–8 mM (70–120 mg dl^{-1}) [1]. Detection and monitoring of glucose in human blood are of great interest in a variety of areas ranging from biomedical applications to ecological approaches. There is a continued high glucose level in diabetic patients as a result of failure to regulate sugar level. Diabetes mellitus is a severe metabolic disorder persistent during the lifetime of a person [2–4]. The pervasiveness of diabetes mellitus has been reported on a global scale, leading to a high rate of blindness, heart disease, and kidney failure worldwide [5]. Gaining appropriate control over the blood glucose level can delay and, to a greater extent, prevent such complications. The key point to develop effective methods for biosensing purposes is to obtain convenient and sensitive signal transductions. Several methods have been extensively employed with the aim of finding reliable approaches for determining glucose levels, including potentiometric biosensors [6, 7], fluorescence spectroscopy [8, 9], calorimetry [10, 11], and electrochemiluminescence [12, 13]. Glycohemoglobin and glucometers test kits are also used in the monitoring and diagnosis of the disease [14, 15]. Although the aforementioned methods are sensitive with high molecular specificity, most of them require expensive instrumentation and trained personnel to operate the devices, and have high maintenance cost.

✉ Ali Farahani
ali_farahani@ut.ac.ir

[1] Department of Chemical Engineering, Queen's University, Kingston, ON K7L 3N6, Canada

[2] Nanobioelectronics Lab, School of Chemistry, College of Science, University of Tehran, Tehran 1748714176, Iran

[3] Department of Chemical Engineering, Faculty of Engineering, University of Tehran, Tehran 1438615995, Iran

POC testing provides highly sensitive and non-invasive systems for continuous, rapid, low-cost, and reliable detection of a variety of biomarkers, such as glucose, in biological samples [16–20]. There is a growing tendency in device miniaturization, especially for electrochemical analysis. In general, reduction of electrode size for electrochemical applications potentially alters the detection sensitivity and accuracy of the method; therefore, providing low-cost procedures along with high-throughput analysis is one the most important aspects of POC testing [21, 22]. Small hand-held devices are developed using state-of-art microfabrication techniques, which automate sample preparation, assay steps, analysis, and detection of signals [23–25].

Diverse electrodes modified with nanomaterials have widely been employed for the development of a wide variety of ultrasensitive electrochemical biosensors, resulting in the drastic improvement in the specificity and stability of the detection systems, achieving reliability and reproducibility. Combination of micro-sized electrodes with nanomaterials is an infrastructure for the development of highly selective biosensors for the future generation of POC tools, resulting in high-throughput analysis as lab-on-chip devices [26–28]. Nanomaterials with high electrical conductivity and large specific area are employed for the modification of electrodes to improve the immobilization of biorecognition agents and facilitate the electron transfer on the electrode surface [29, 30]. Oriented nanomaterials can improve the biorecognition efficiency and decrease the nonspecific adsorption of the molecules, significantly enhancing the sensitivity for the detection of the target analyte.

Owing to their great optical, electrical, and mechanical properties, single-walled carbon nanotubes (SWCNTs) are versatile materials for electrochemical sensing [31]. Their high specific surface area, easy functionalization, and high electroconductivity, along with facile non-covalent adsorption of molecules via π–π interactions, make them unique materials for biosensing applications [32]. Moreover, due to their terminal activation, it is possible to assemble SWCNTs to form oriented nanostructures [33]. Vertically oriented carbon nanotubes, either in random distribution or in a regular pattern, have shown promising features mainly in the areas of energy-saving, sensing, and biosensing [34–37]. These entities combine the properties of microelectrode arrays and carbon nanotubes. Thanks to their high surface area and conductivity, each of the arrays can act as a means for direct electron transfer between the electrode and the receptor. The main advantage of the arrays is the increase in current density, mass transport rate, and enhancement in signal-to-noise ratio, which are mainly due to the formation of three-dimensional diffusion fields and less ohmic resistance effects [27, 38]. As a result, aligned carbon nanotubes can be employed as efficient molecular wires to facilitate the heterogeneous electron transfer between the electrodes and the surrounding environment [39]. The structural arrangement of SWCNTs can also allow the complete exposure of their sidewalls, improving the non-covalent adsorption of molecules and detection efficiency. A wide range of biochemical applications has been demonstrated for VACNTs in the presence or absence of encapsulating materials, such as glucose detection [40], tracking gene delivery [41], and electrochemical detection of dopamine [42]. Furthermore, their properties such as wide electrochemical potential window, high thermal and electrical conductivity, and high mechanical stability make them competitive candidates for covalent attachment of enzymes, avoiding the degradation of the enzyme on the substrate, and contribute to better electron transfer between electrode and redox center of the enzyme [43–45]. Aligned carbon nanotubes have been used as a platform for the covalent attachment of molecules to generate a lab-on-chip system based on CNT arrays. As integrated platforms, these devices can collect and analyze data and play a unique role in the development of portable devices [46, 47].

This research describes an efficient method for low potential, mediator-less determination of glucose by covalent attachment of GOx on VACNTs. The as-prepared biosensor is applied for the low-cost, rapid, and accurate detection of glucose in a wide concentration range. To the best of our knowledge, this is the first report on the development of a POC device that combines carbon nanotube arrays with a miniature potentiostat integrated with a microfluidic chamber. The designed system is capable of performing real-time measurements and selective determination of glucose in the presence of ascorbic acid (AA) and uric acid (UA) in biological samples.

Experimental

Chemical and reagents

Glucose oxidase (G7141-50KU), D-(+)-glucose, 1-(3-dimethylamino propyl)-3 ethyl carbodiimide hydrochloride (EDC), N-hydroxysulfosuccinimide sodium salt (sulfo-NHS), potassium ferricyanide ($K_3[Fe(CN)_6]$), uric acid (UA), ascorbic acid (AA), KH_2PO_4, K_2HPO_4, and bovine serum albumin (BSA) were purchased from Sigma-Aldrich (Saint Louis, MO). Plasma samples were obtained from the Iranian Blood Transfusion Organization (Tehran, Iran). Other chemicals and reagents were of analytical grade and purchased from Merck (Darmstadt, Germany). All solutions were prepared with double-distilled water, immediately before each experiment. Phosphate-buffered solution (PBS), pH 7.0, was used as the supporting electrolyte.

Equipment

The CV and amperometric measurements were performed with an Ivium Palmsens 2 (Houten, Netherland) for primary tests in a three-electrode setup using VACNTs as the working

electrode, an Ag/AgCl (Azar electrode, Urmia, Iran) as the reference electrode, and a platinum wire as the counter electrode. Radio frequency sputtering (EVS200—135 W) and electron beam evaporation (Veeco Co—135 W) were employed for the deposition of alumina (Al_2O_3) and iron (Fe), respectively. Electrochemical impedance spectra were obtained with a CHI 660 electrochemical workstation (CH Instruments, Austin, TX). FESEM (FEI NOVANANOSEM 450) (Hitachi, Santa Clara, CA) and ATR-FTIR (Tensor 27, Equinox 55, attenuated Bruker, Karlsruhe, Germany) were used to characterize the morphology of the VACNTs.

Point of care analyzer

The POC device consisted of four main parts, including (a) VACNT electrode, (b) a microfluidic chamber, (c) two syringe pumps, and (d) a miniature potentiostat.

VACNT electrode

Prior to the growth of VACNTs, the silicon substrate (Si/SiO_2) was rinsed twice using deionized water and dried completely. Al_2O_3 film with a thickness ranging between 10 and 20 nm was deposited on the substrate using radio frequency under a vacuum of 8 Torr. Fe was deposited as the catalyst on Al_2O_3 with a thickness of 10 nm using electron beam evaporation under the vacuum of 10 Torr. Prior to the growth process of arrays, thermal annealing at the presence of argon flow was carried out at the temperature of 600 °C. VACNTs with an average length of 9 μm and diameter ranging between 70 and 100 nm were grown on Fe sites, well separated from each other. The arrays' growth occurred in a mixture of H_2/C_2H_4 (90/60 sccm) at the temperature of 600 °C. The reaction was carried out for the desired time before the ethylene and hydrogen flow were cut off. The argon flow was not cut off until the temperature was reduced to room temperature. After CNT arrays' growth, the produced chip was washed in dilute HNO_3 solution, resulting in the removal of loose particles as well as purification of the arrays.

Microfluidic chamber

A custom-made microfluidic chip was designed to accommodate the fabricated biosensor for performing electrochemical measurements (see Supplementary Information (ESM) Fig. S1). The chip was placed in series with syringe pumps to allow precise and repeatable measurements in the microliter scale. The electrode was placed between two polydimethylsiloxane (PDMS) blocks. The lower part includes appropriate margins to position the electrode and an O-ring to seal the upper surface. The sample is mixed with the buffer in a serpentine, mixing channel before being introduces into the test chamber in a polyethylene tube.

Syringe pump

Two custom-made, low-cost, miniaturized syringe pumps for precise dispensing and withdrawal of sample solutions were made using open-source electronic hardware (Arduino Uno) and 3D printed parts. The pumps were controlled by an Arduino interface and the precise stepper motor driver kit DRV8825.

Miniature potentiostat

The gas sensor LMP91000 (Texas Instrument, TX) (ESM Fig. S2a) acts as a two-electrode system in tandem with a modified microcontroller (Arduino, Italy) (ESM Fig. S2b). The evaluation board on the LMP91000 is a field-programmable gate array (FPGA)-based device which can control the LMP91000 via USB, and an interface named sensor AFE (Texas Instrument, TX), which can manually control the board. This board needs an external card (data acquisition card) for capturing the generated analog signals. Although the board can be programmed manually to perform CV, constant sampling rate is not achievable. Moreover, the use of an external FPGA will also increase the cost and size of the device. To solve this issue, an Arduino Due based on an 84 MHz, ARM microcontroller was added to the system, and LMP was powered and controlled via the I2C interface. The LMP was reconfigured to be able to perform CV and amperometry measurements. The board generates a voltage which is proportional to the current from the working electrode.

At the output level, the voltage is provided by a transimpedance amplifier (TIA), which converts the current to voltage; then, the response is sent to Arduino using a serial peripheral interface)SPI). For the ADC (analog to digital converter) unit, the LMP9100EVM setup should be manually adjusted to allow precise calculation of the output.

The transimpedance amplifier can act at different amplification levels, thus allowing the gain to match the analyte concentration range; for example, since the current is proportional to the concentration of the target analyte, a higher gain can be selected for lower analyte concentrations.

The performance of LMP91000 at the voltage range of 2.5 V makes it possible to do CV and amperometry analysis at various ranges. The output voltage of LMP91000 is proportional to the current between electrodes. Based on Eq. 1, calibration of the system can be done by making changes in concentrations and embedded transfer function.

$$I_{\text{out}} = (V_{\text{out}} - V_{\text{int}}z)/\text{TIA}_{\text{gain}} \quad (1)$$

The MATLAB and Simulink R2016-b software were utilized for all data savings and calibrations. The LMP91000EVM was reconfigured to perform CV measurements on the three-

electrode systems. The obtained data is stored in the SD card of the Arduino. Figure 1 shows the POC system for the detection of glucose.

System testing and validation

As mentioned earlier, the potentiostat performance was evaluated, and the parameters were adjusted for each experiment manually. The device successfully performs CV measurements. The data could be stored in Arduino using a data logger shield, or it could be transferred to a PC using Bluetooth module. The validation of the measurements was also carried out using a commercial potentiostat (Palmsens 2) for Fe(II)/Fe(III) redox in PBS buffer. Fig. S3 (see ESM) shows the results from both potentiostats depicting sharp and well-defined oxidation-reduction peaks.

Enzyme immobilization

To expose the contact layer of the arrays, prior to the enzyme immobilization, the electrode was treated with a 10% HF solution. To generate carboxylic functional groups (COOH) at the CNT tips, and, consequently, covalent binding of GOx enzyme to them, the VACNTs were pretreated with 1.5 M NaOH at 1 V for 60 s. Next, in order to promote the amide cross-linkage between the activated tips and GOx, the arrays were immersed in PBS (pH = 7.0, 0.1 M) containing 10 mg/ml EDC and 30 mg/ml NHS. Then, a 0.5-ml drop containing enzyme solution (5 mg/ml) was placed on the electrode surface, and the reaction was allowed to take place for 2 h. Following the immobilization, the electrode was carefully washed in PBS solution (pH = 7.0) containing 0.3% wt BSA and stored at 4 °C before use. Figure 2 is a schematic illustrating the enzyme immobilization of CNT tips.

Real sample pretreatment

The human blood plasma samples were acquired from healthy and diabetic volunteers with approved permission from the Iranian Blood Transfusion Organization (Tehran, Iran). One milliliter of four aliquots of each sample was transferred to four separate test tubes; three of the aliquots were spiked with different concentrations of glucose. Spiked and unspiked samples were diluted in 2 ml of MeOH to remove the proteins. Following protein removal, samples were sonicated for 1 min and centrifuged for 7 min at 6000 rpm. After filtering the supernatants with paper filters, 3 ml of PBS was added to adjust pH to 7.

Results and discussion

Morphological characterization of VACNTs

Figure 3A and B are the FESEM images of as-grown VACNTs depicting the of arrays' morphology. Owing to the van der Waals attraction forces and large surface area on nanotubes [48], the arrays make a well-ordered structure. The diameters of the arrays measured by ImageJ software (version 1.51, LOCI, University of Wisconsin(were in the range of 70–100 nm, while the mean tube length was 9 μm. Since the dimensions of walls of the oriented arrays were comparable with the size of glucose oxidase, the latter can be covalently attached to the tips and walls of the arrays. Figure 3C shows the FESEM image of CNT arrays after functionalization with NaOH. Comparing with Fig. 3B, it seems that functionalization did not result in severe shortening and cutting of nanotubes. Figure 3D shows the distribution of the CNT diameters in the arrays, and as mentioned earlier, the diameter is between 70 and 100 nm.

FTIR was utilized to explain the crystalline nature of CNT arrays. In Fig. 3E (line "(a)"), 1750 cm^{-1} is the C–O stretching

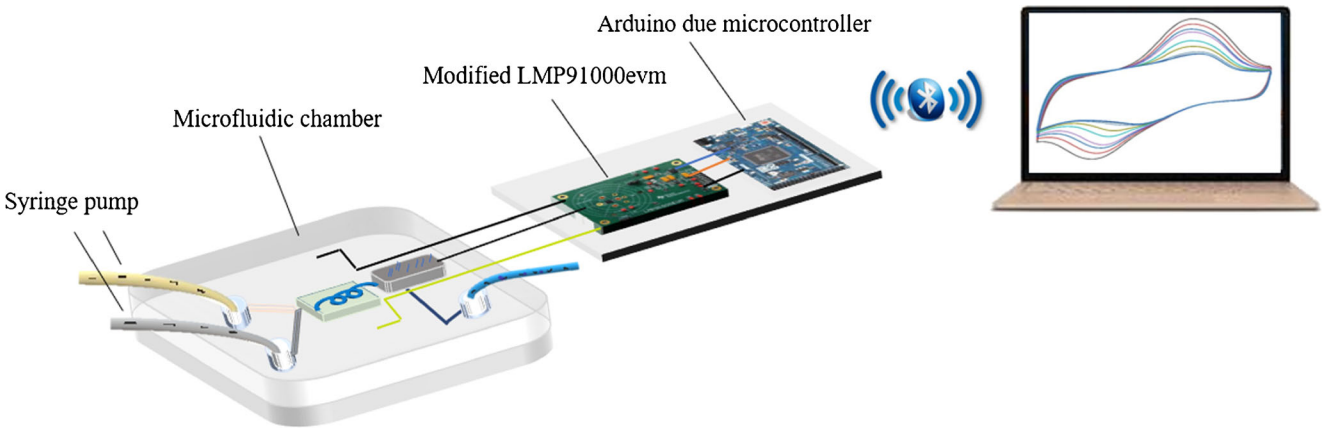

Fig. 1 Point of care system for detection of glucose

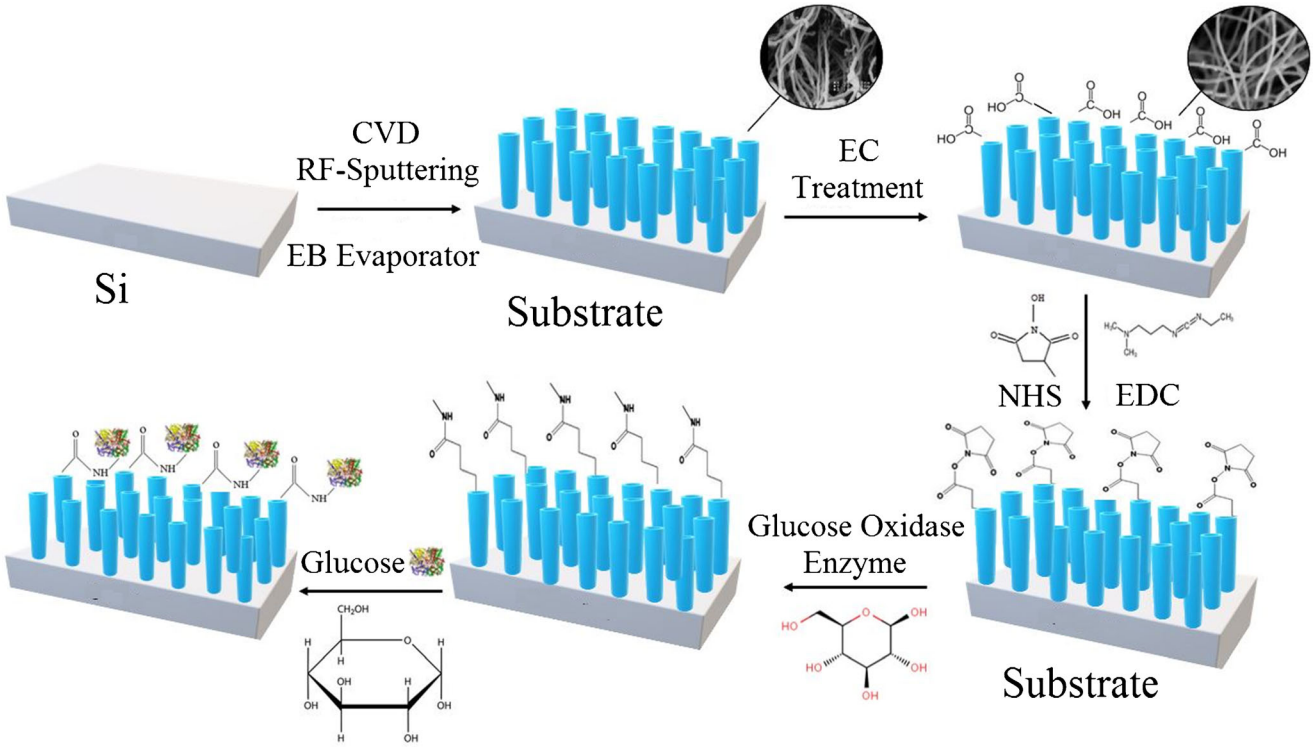

Fig. 2 Schematic of the immobilization steps on the electrode surface

vibration and 3467 cm^{-1} is the –OH vibration of the carboxyl group. As can be seen in Fig. 3E (line "(b)"), the intensity of carboxyl groups has increased after chemical treatment, which indicates the successful functionalization of the arrays. The band at 2950 cm^{-1} is assigned to aliphatic C–H stretching vibrations on the electrode surface. Presence of functional groups enhances the amide linkage between the amine residues of the enzyme and activated electrode surface.

Electrochemical characterization of VACNT electrode

Effect of scan rate and EIS

Immobilization of GOx on the electrode was confirmed by the detection of the derived redox peaks due to GOx immobilization. CV and EIS were directed to assess the electrochemical properties of VACNTs. Cyclic voltammograms of the electrode at different scan rates (10–450 mV/s) taken in PBS (pH 7.0, 0.1 M) are given in Fig. 4a. To verify the nanoscale behavior of the arrays, their CV must have a sigmoidal shape, showing the steady-state mass transfer in the slow scan rates. For the scan rates between 10 and 180 mV/s, there is a linear relationship between oxidation ($R^2 = 0.995$) and reduction ($R^2 = 0.994$) peak currents and the square root of scan rates (Fig. 4b), proving that the electrochemical process is controlled by linear diffusion of electroactive species. At the same scan rate, the reduction peak is almost equal to the oxidation peak. As the scan rate increases, the oxidation peak shifts to more positive values and the reduction peak shifts to more negative values. Moreover, with the increase in scan rate ΔE_p gradually, all which shows the electron transfer of the electrode is quasi-reversible. Sigmoidal voltammogram of the resultant arrays can be described by spherical diffusion of the arrays, which prevents overlapping of the neighboring arrays.

Figure 4c shows impedance spectra of VACNT electrode at the solution of 4 mM $K_3Fe(CN)_6$/4 mM $K_4Fe(CN)_6$ and 0.1 M KCl in PBS (pH 7.0, 0.1 M) (1:1 mixture). The impedance spectra of the electrode appeared as a straight line, showing the linear diffusion-controlled behavior of the system. The impedance spectra are meaningful only if the response is independent of the amplitude plot. So, there would be no change with the amplitude with the voltage variation. According to the impedance spectra, the system maintains its linearity even at high amplitudes, indicating that the electrode is a good candidate for high amplitude EIS studies.

Glucose detection

The activity of the enzymatic biosensors is highly dependent on experimental parameters, including temperature, pH, and concentration of the coenzyme. After optimization [37], the best performance of the electrode was achieved at a PBS pH 7.0, a temperature of 25 °C, and a concentration of 2.5 mM of flavin adenine (FAD).

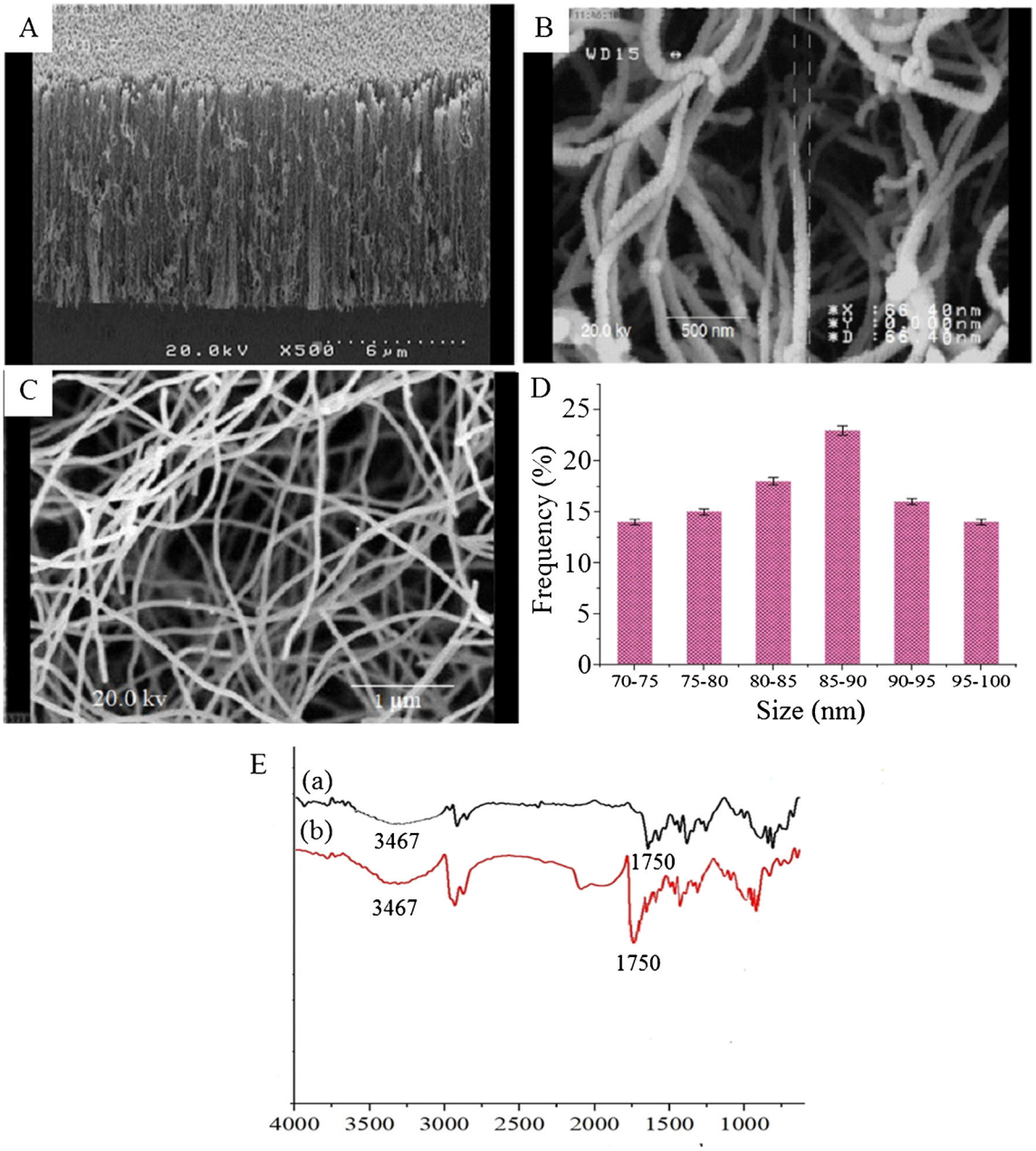

Fig. 3 (A, B) SEM images of VACNTs. (C) SEM image of VACNTs after chemical treatment. (D) The histogram of array's diameter distribution. (E) ATR-FTIR spectra of VACNTs before (a) and after (b) chemical treatment

The miniature sensor was employed to detect glucose by means of electrochemical analysis. In order to study the electroanalytical activity of the electrode toward glucose detection, CV measurements were carried out in PBS pH 7.0 containing 2.5 mM FAD in the absence and presence of 2 mM of glucose. GOx enzyme was covalently attached to the tips of VACNTs. GOx catalyzes the oxidation of glucose in the presence of dissolved oxygen, producing gluconolactone and H_2O_2 simultaneously (Eqs. 2 and 3). To perform as a catalyst, GOx cooperated with FAD as a redox cofactor. FAD is an electron acceptor and is reduced to $FADH_2$.

After the oxidation of H_2O_2 (Eq. 4), the electrode recognizes the number of electron transfers, which is relevant to the number of glucose molecules in standard and real samples.

$$\text{Glucose} + \text{GOx}{-}\text{FAD}^{+} \rightarrow \text{Gluconolactone} + \text{GOx}{-}\text{FADH}_2 \quad (2)$$

$$\text{GOx}{-}\text{FADH}_2 + \text{O}_2 \rightarrow \text{GOx}{-}\text{FAD} + \text{H}_2\text{O}_2 \quad (3)$$

$$\text{H}_2\text{O}_2 \rightarrow 2\text{H}^{+} + \text{O}_2 + 2\text{e} \quad (4)$$

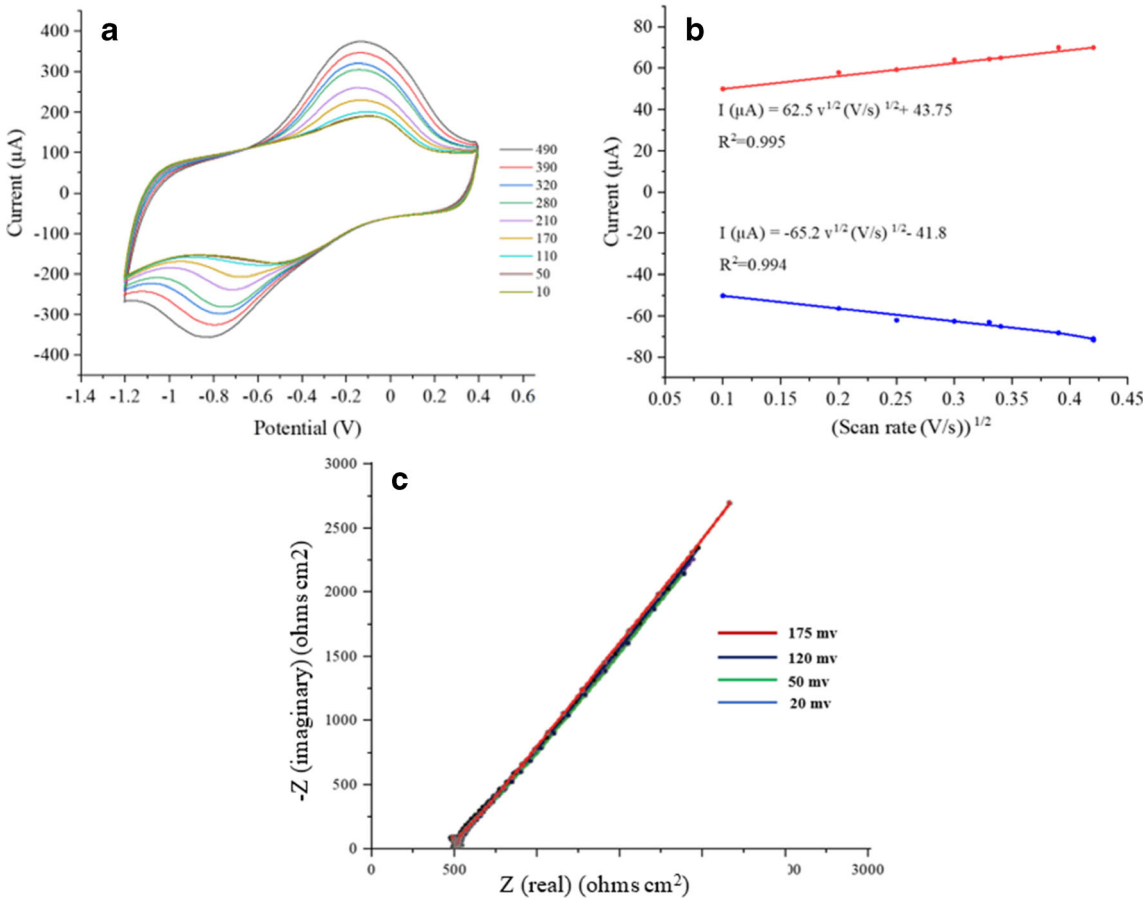

Fig. 4 **a** Cyclic voltammogram of GOx/VACNTs in PBS pH 7.0 at scan rates between 10 and 450 mVs^{-1}. **b** Calibrated plots of peak currents vs. square root of scan rate in the range of 10–180 mVs^{-1}. **c** Impedance spectra of VACNT electrode at the solution of 4 mM $K_4Fe(CN)_6$/4 mM $K_3Fe(CN)_6$ and 0.1 M KCl in PBS (pH 7.0, 0.1 M) (1:1 mixture). The spectra were taken at 0.5 Hz to 120 kHz

As shown in Fig. 5a, following glucose addition, the anodic peak current becomes considerably higher, and the cathodic peak lower, indicating the electrode's excellent electrocatalytic activity for direct electrode transfer of glucose.

The selective detection of glucose in the presence of other interferences by the dehydrogenase-based biosensor can be effectively achieved when the electro-oxidation of $FADH_2$ is performed at less anodic potentials. Figure 5b shows the amperometric-response curve of the electrode toward successive addition of glucose in 5 ml of PBS solution at the potential of − 0.55 V. Upon injection of glucose, there is a stepwise increase at the current of electrocatalytic oxidation of glucose which reaches a stable state with uniform increments. In this process, H_2O_2 is detected, resulting from the oxidation of glucose in the presence of glucose oxide. The average time to produce a steady-state current in each step was found to be 10 s, meaning that the device can be used as a fast-response glucose biosensor. Figure 5c shows the calibration curve (current vs. concentration) for glucose oxidation.

Based on the slope of the calibration curve, the fabricated biosensor had a sensitivity of 1462 μA mM^{-1} cm^{-2} and 1015 μA mM^{-1} cm^{-2} at the linear range of 1.2–7.8 μM and 7.8–11.2 μM, respectively. The detection limit was estimated to be 23 μM (based on the signal-to-noise ratio (*S*/*N*) of 3). The high sensitivity of the glucose biosensor can be attributed to the high surface area of the electrode, providing the glucose with better access to active sites of glucose oxidase.

The higher sensitivity observed at lower concentrations of glucose can be explained by the fact that due to the enhancement of diffusive effects at low substrate level, even a small concentration change results in a considerable change in the electrode response. Moreover, at low glucose level, the local concentration is quickly depleted at the electrode surface as GOx changes substrate into product, resulting in high sensitivity toward target molecule detection. At higher glucose concentration, GOx has been immobilized on the electrode surface for a more extended time window and reaction proceeds over a longer period of time. Furthermore, possibility of surface fouling by the products justifies the lower slope at higher glucose concentration. To confirm the sensing ability of the biosensor in real samples, the glucose prepared in human plasma (100 nM) was added to PBS. Based on Fig. 5d, the biosensor could only detect glucose in human plasma, and

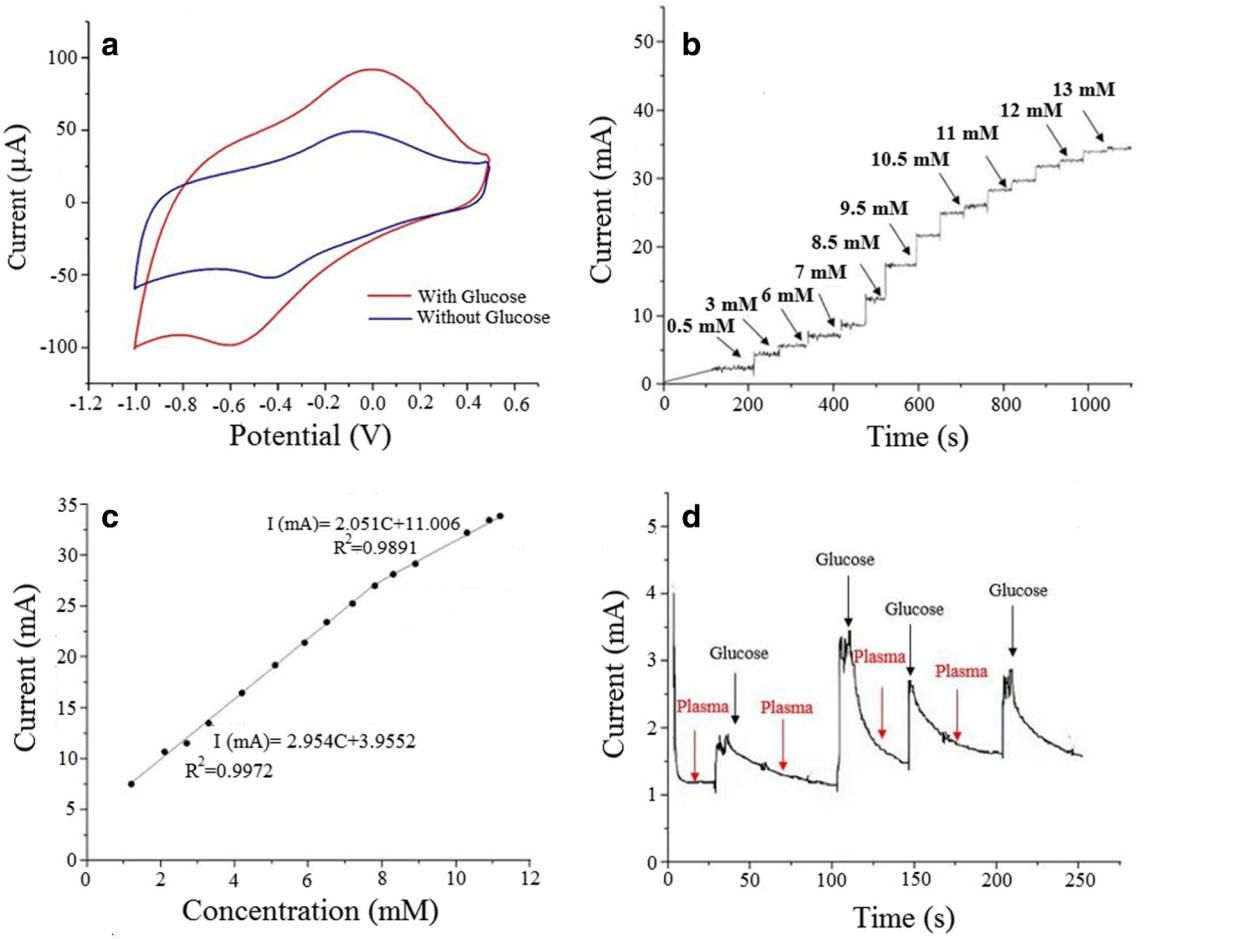

Fig. 5 **a** Voltammogram of the biosensor response in PBS solution containing 2.5 mM of FAD^+ in the absence and presence of 2 mM glucose. **b** Amperometry response of the electrode to successive addition of glucose at the potential of − 0.55 V in PBS, pH 7.0 containing 2.5 mM of FAD^+. Concentration of glucose after each addition was 0.5, 01, 2, 3, 4, 5, 6, 7, and 8 mM. **c** The calibration curve corresponding to different glucose concentrations. **d** Sensitivity of biosensor for real sample analysis

there was no response when it was added to sample without glucose.

The surface area and diffusion coefficient of the glucose can be calculated using the Cottrell equation (Eq. 5), which describes a linear relationship between I and $t^{-1/2}$.

$$I = \frac{nFAD^{1/2}C}{\pi^{1/2}} t^{-1/2} \quad (5)$$

where A and D are the surface area and diffusion coefficient of glucose, respectively. Based on the slope of Fig. 6, and regarding $n = 1$ and $D = 7.6 \times 10^{-8}$ cm^2/s, the effective surface area of the electrode is calculated to be approximately 0.024 cm^2.

Electrochemical interference analysis

In addition to glucose, human blood contains molecules such as AA and UA, which their oxidation can interrupt selective glucose detection. Consequently, the selectivity of the glucose

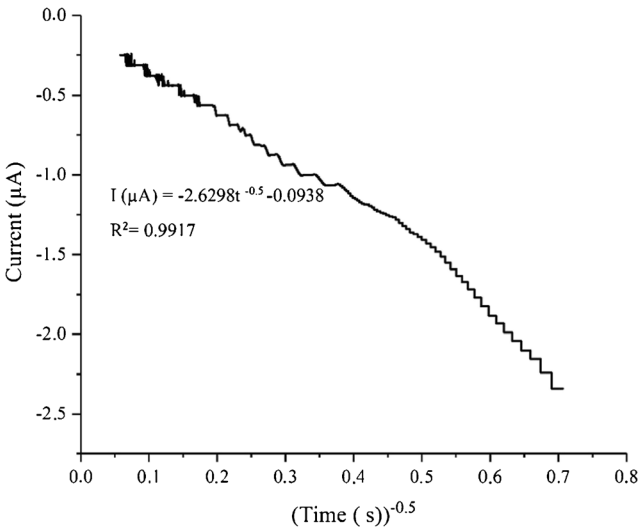

Fig. 6 I vs. $t^{-0.5}$ for amperometry response of the electrode toward addition of glucose

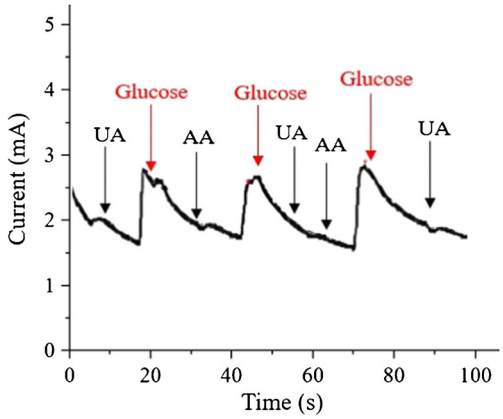

Fig. 7 Selectivity of the electrode toward glucose detection at the presence of UA and AA interferences

sensor is of great importance. The average level of glucose in blood serum is between 4 and 8 mM, while the average level of these interferences is no more than 0.1 mM. Figure 7a shows the response of the electrode upon the addition of 2.0 mM glucose, 0.1 mM AA, and 0.1 mM UA in PBS pH 7.0, at the potential of − 0.55 V. Following the addition of 2.0 mM glucose, there was a significant rise in amperometric current response, while the addition of 0.1 mM of UA and AA caused no change in the amperometric response. The results showed that regardless of the co-existence of major interferences, the fabricated electrode is highly selective toward the glucose detection.

Stability and reproducibility of the electrode

Long-term stability of VACNTs/GOx is assessed by analyzing its anodic peak current in the mixture of 2.0 mM glucose in PBS pH 7.0, temperature of 25 °C, and intervals of every 5 days in 60 days. As shown in Fig. 8a, the current of the electrode retains 88% of the initial current response after 60 days, revealing good mechanical stability of the electrode, which is due to the characteristics of VACNTs and proper immobilization of GOx on the surface of the electrode. Moreover, the electrode retains more than 80% of its initial faradic current after 60 days. The results indicate that the structural stability of the biosensor is suitable for analytical purposes.

To evaluate the reproducibility in the manufacturing of the POC devices, eight batches of VACNTs/GOx electrodes were studied under the same experimental conditions (− 1 to 0 V potential window in PBS of pH 7.0 temperature of 25 °C, containing 2 mM glucose). The results (Fig. 8b) exhibit that the anodic peak currents on the CVs are close to each other (the calculated RSD was 1.75%) presenting a satisfactory reproducibility of the electrode.

Real sample analysis

One of the critical attributes of the glucose biosensor is the ability to distinguish between glucose and interference species such as UA and AA that coexist in the blood. Besides, its feasibility for the practical application was further investigated by real sample analysis by standard addition method. Plasma samples from healthy volunteers were obtained from the Iranian Blood Transfusion Organization (Tehran, Iran) and stored at − 20 °C until use and another sample was also obtained from a diabetic patient tested after pretreatment procedure. The tests were not done for 7 to 10 mM, for diabetic patient due to the fact that these levels were out of linear range and possibly not happen in real conditions. Based on Table 1, all relative standard deviations (RSDs) are less than 6% and

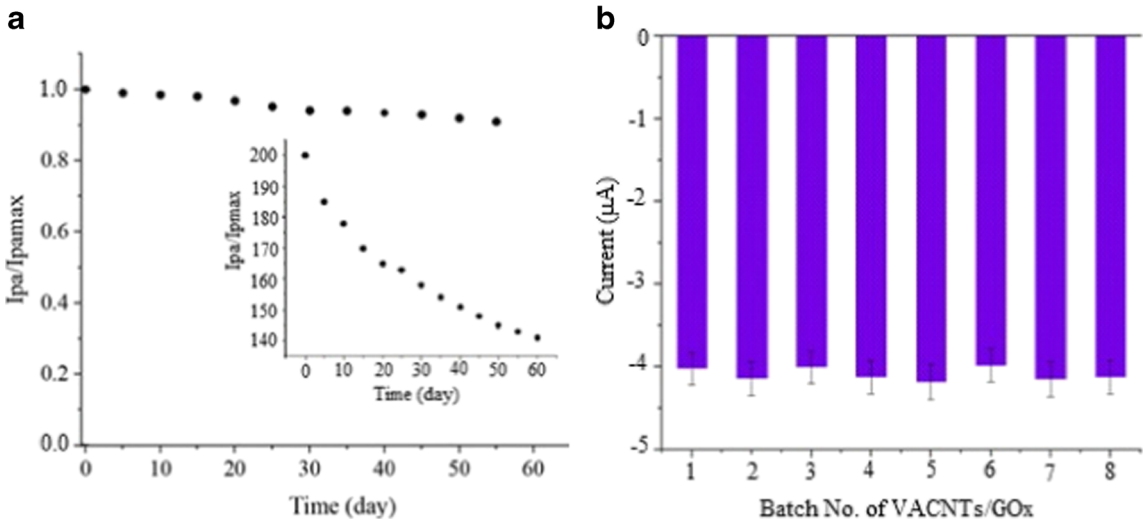

Fig. 8 **a** Anodic peak current of VACNT/GOx electrode monitored every 5 days. Inset: the faradic component of anodic current on the electrode. **b** Average anodic peak current of the VACNTs/GOx electrode assembled in five batches

Table 1 Real sample analysis in human blood plasma

Sample	Spiked (mM)				Found ± RSD % (mM) ($n = 3$)			
Human Plasma1[a]	0	4	7	10	nd[c]	3.91 (± 0.12)	7.03 (± 0.43)	10.0 (± 0.49)
Human Plasma2[a]	0	4	7	10	nd[c]	3.96 (± 0.16)	6.99 (± 0.25)	9.9 (± 0.34)
Human Plasma3[a]	0	4	7	10	nd[c]	4.07 (± 0.25)	7.02 (± 0.43)	10.0 (± 0.23)
Human Plasma4[b]	0	4	-	-	7.13 (± 0.11)	11.3 (± 0.34)	-	-

[a] Sample from a healthy volunteer. [b] Sample from diabetic patient. [c] Not detected

relatively close to the spiked amounts, demonstrating that the electrode is capable of detecting glucose in human plasma samples with an acceptable level of accuracy.

Comparison with other methods

Performance and analytical characteristics of the biosensor along with some other electrodes are summarized in Table 2. In comparison to other methods, the developed biosensor has a higher sensitivity, a comparable limit of detection, and an appropriate linear detection range with respect to glucose concentration in human blood plasma. The results also demonstrate that the biosensor is highly selective toward glucose at the presence of interferences. Moreover, compared to other methods, fabrication of developed biosensor is easier and less expensive, providing a miniaturized, cost-effective, and portable system for accurate detection of glucose in biological samples, which even non-experienced people can use for analytical purposes.

Performance and analytical characteristics of the biosensor along with some other electrodes are summarized in Table 2.

Conclusion

In summary, a novel, portable diagnostic device based on VACNTs was developed and successfully applied for the detection of glucose in human blood plasma samples (RSD < 6%). By integrating a micro-size biosensor, a low-cost potentiostat, and a miniature syringe pump in tandem with a microfluidic chamber, a POC assembly was achieved and applied for determining glucose in biological samples. The results of FESEM and EIS analysis confirm the desired characteristics of the biosensor. Owing to the efficient electron transfer, based on the amperometric results, the fabricated electrode has a low detection limit of 23 μM ($S/N = 3$), sensitivity of 1462 μA mM^{-1} cm^{-2} at the linear range of 1.2–7.8 μM, and sensitivity of 1015 μA mM^{-1} cm^{-2} at the linear range of 7.8–11.2 μM. In addition, it has the advantages of anti-interference capability, high reproducibility (RSD = 1.75%), and good stability. Considering the urgent need for available and reliable miniature systems, our biosensor is compatible with miniaturized systems and is a potential detection platform for POC testing.

Table 2 Comparison of the analytical parameters of the VACNTS/GOx electrode with some other glucose biosensors

Electrode	Detection E (V)[1]	LDR (mM)	Detection limit (μM)	Sensitivity (μA/mM/cm^2)	Detection method	Ref
GOx-GO-SH-Au-SPE	-	3–9	319.4	3.17	CV	[49]
GOx/Pt/rGO/P3ABA/SPE	0.5	0.25–6	44.3	22.01	Amperometry	[50]
Polyacrylonitrile/Au/GOx/CNT	− 0.45	1–30	4	0.47	Amperometry	[51]
PTTzFr/GOx on graphite	− 0.7	0.005–0.7	0.012.8	65.44	Amperometry	[52]
(CS-GLM)7-GCE	-	0.01–10	1.31	-	CV	[53]
PAA-rGO/VS-PANI/LuPc2/GOx-MFH	0.3	2–12	25	15.31	Amperometry, CV	[54]
GOx/Pt-MWCNTs/CSF	0.65	0–5	50	288.86	Amperometry, CV	[55]
Chitosan/GOx/gold	0.4	1–20	1.83	580	CV	[56]
PdNi@rGO	0.5	0.025–12	0.052	40.9	CV	[57]
VACNTs/GOx	− 0.55	1.2–7.8 7.8–11.2	23	1462 1015	CV	This work

[1] At lower potentials, the possibility of oxidation of interference is less than at higher potentials, which results in higher selectivity

Supplementary Information The online version contains supplementary material available at https://doi.org/10.1007/s00216-020-03108-3.

Compliance with ethical standards

Conflict of interest The authors declare that they have no conflicts of interest.

Informed consent The human plasma samples were obtained from healthy and diabetic patient volunteers with informed consent to the Iranian Blood Transfusion Organization (Tehran, Iran). The studies have been performed in accordance with the ethical standards approved by the appropriate research ethics committee of the University of Tehran.

References

1. Scognamiglio V. Nanotechnology in glucose monitoring: advances and challenges in the last 10 years. Biosens Bioelectron. 2013;47:12–5.
2. McIntyre HD, Catalano P, Zhang C, Desoye G, Mathiesen ER, Damm P. Gestational diabetes mellitus. Nat Rev. 2019;5(1):1–19.
3. Vu N, Narvaez-Rivas M, Chen GY, Rewers MJ, Zhang Q. Accurate mass and retention time library of serum lipids for type 1 diabetes research. Anal Bioanal Chem. 2019;411(23):5937–49.
4. Hussain S, Park SY. Optical glucose biosensor based on photonic interpenetrating polymer network with solid-state cholesteric liquid crystal and cationic polyelectrolyte. Sens. Actuators, B. 2020:128099.
5. Muscatello MMW, Stunja LE, Asher SA. Polymerized crystalline colloidal array sensing of high glucose concentrations. Anal Chem. 2009;81:4978–86.
6. Wahab HA, Salama AA, El Saeid AA, Willander M, Nur O, Battisha IK. Zinc oxide nano-rods based glucose biosensor devices fabrication. Results Phys. 2018;9:809–14.
7. Guadarrama-Fernández L, Novell M, Blondeau P, Andrade FJ. A disposable, simple, fast and low-cost paper-based biosensor and its application to the determination of glucose in commercial orange juices. Food Chem. 2018;265:64–9.
8. Benito-Peña E, Valdés MG, Glahn-Martínez B, Moreno-Bondi MC. Fluorescence based fiber optic and planar waveguide biosensors. A review Anal Chim Acta. 2016;943:17–40.
9. Bobrowski T, Schuhmann W. Long-term implantable glucose biosensors. Curr Opin Electrochem. 2018;10:112–9.
10. Wang Z, Kimura M, Ono T. Manufacturing and characterization of simple cantilever thermal biosensor with Si-metal thermocouple structure for enzymatic reaction detection. Thermochim Acta. 2018;668:110–5.
11. Fei R, Means AK, Abraham AA, Ak L, Coté GL, Grunlan MA. Self-cleaning, thermoresponsive P (NIPAAm-co-AMPS) double network membranes for implanted glucose biosensors. Macromol. Mater. Eng. 2016;301(8):935–43.
12. Tian K, Nie F, Luo K, Zheng X, Zheng J. A sensitive electrochemiluminescence glucose biosensor based on graphene quantum dot prepared from graphene oxide sheets and hydrogen peroxide. J Electroanal Chem. 2017;801:162–70.
13. Xiao Y, Xu L, Qi LW. Electrochemiluminescence bipolar electrode array for the multiplexed detection of glucose, lactate and choline based on a versatile enzymatic approach. Talanta. 2017;165:577–83.
14. Lisi F, Ariotti N, Bakthavathsalam P, Benedetti T, Tilley RD, Gooding JJ. The use of a personal glucose meter for detecting procalcitonin through glucose encapsulated within liposomes. Analyst. 2019;144(21):6225–30.
15. Chidri SV, Vidya G. Assessment of pulmonary functions in type 2 diabetes mellitus: its correlation with glycemic control and body mass index. Natl J Physiol Pharm Pharmacol. 2020;10(7):553–6.
16. Thaler M, Luppa PB. Highly sensitive immunodiagnostics at the point of care employing alternative recognition elements and smartphones: hype, trend, or revolution? Anal Bioanal Chem. 2019:1–13.
17. Farahani A, Sereshti H. An integrated microfluidic device for solid-phase extraction and spectrophotometric detection of opium alkaloids in urine samples. Anal Bioanal Chem. 2020;412(1):129–38.
18. Farahani A, Azimi S, Tajaddodi A, Docoslis A, Tashakori C. Screen-printed anion-exchange solid-phase extraction: a new strategy for point-of-care determination of angiotensin receptor blockers. Talanta. 2020;222:121518.
19. Mercer C, Bennett R, Conghaile PÓ, Rusling JF, Leech D. Glucose biosensor based on open-source wireless microfluidic potentiostat. Sensors Actuators B Chem. 2019;290:616–24.
20. Gao J, Huang W, Chen Z, Yi C, Jiang L. Simultaneous detection of glucose, uric acid and cholesterol using flexible microneedle electrode array-based biosensor and multi-channel portable electrochemical analyzer. Sensors Actuators B Chem. 2019;287:102–10.
21. Zarei M. Advances in point-of-care technologies for molecular diagnostics. Biosens Bioelectron. 2017;98:494–506.
22. Syedmoradi L, Daneshpour M, Alvandipour M, Gomez FA, Hajghassem H, Omidfar K. Point of care testing: the impact of nanotechnology. Biosens Bioelectron. 2017;87:373–87.
23. Farahani A, Sereshti H. Developing a point-of-care system for determination of dopamine, ascorbic and uric acids in biological fluids using a screen-printed electrode modified by three dimensional graphene/carbon nanotube hybrid. Int J Electrochem Sci. 2019;14:6195–208.
24. Kumar S, Rani R, Dilbaghi N, Tankeshwar K, Kim KH. Carbon nanotubes: a novel material for multifaceted applications in human healthcare. Chem Soc Rev. 2017;46(1):158–96.
25. Chen J, Meng HM, An Y, Liu J, Yang R, Qu L, et al. A fluorescent nanosphere-based immunochromatography test strip for ultrasensitive and point-of-care detection of tetanus antibody in human serum. Anal Bioanal Chem. 2020;412(5):1151–8.
26. Pourahadi A, Farahani A, Hosseiny Davarani SS, Nojavan S, Tashakori C. Developing a miniaturized setup for in-tube simultaneous determination of three alkaloids using electromembrane extraction in combination with ultraviolet spectrophotometry. J Sep Sci. 2019;42(19):3126–33.
27. Wang C, Wang Y, Zhou Y, Wu ZQ, Xia XH. High-performance bioanalysis based on ion concentration polarization of micro-/nanofluidic devices. Anal Bioanal Chem. 2019:1–10.
28. Yoon H, Nah J, Kim H, Ko S, Sharifuzzaman M, Barman SC, et al. A chemically modified laser-induced porous graphene based flexible and ultrasensitive electrochemical biosensor for sweat glucose detection. Sensors Actuators B Chem. 2020;311:127866.
29. Bilal M, Zhao Y, Rasheed T, Iqbal HM. Magnetic nanoparticles as versatile carriers for enzymes immobilization: a review. Int J Biol Macromol. 2018;120:2530–44.
30. Farzin L, Shamsipur M. Recent advances in design of electrochemical affinity biosensors for low level detection of cancer protein biomarkers using nanomaterial-assisted signal enhancement strategies. J Pharm Biomed. 2018;147:185–210.
31. Wang Z, Dai Z. Carbon nanomaterial-based electrochemical biosensors: an overview. Nanoscale. 2015;7(15):6420–31.
32. Yang R, Tang Z, Yan J, Kang H, Kim Y, Zhu Z, Tan W. Tan, Noncovalent assembly of carbon nanotubes and single-stranded DNA: an effective sensing platform for probing biomolecular interactions. Anal Chem 2008;80(19):7408–7413.
33. Rawson FJ, Yeung CL, Jackson SK, Mendes PM. Tailoring 3D single-walled carbon nanotubes anchored to indium tin oxide for

natural cellular uptake and intracellular sensing. Nano Lett. 2013;13(1):1–8.
34. Aydinli A, Yuksel R, Unalan HE. Vertically aligned carbon nanotube–Polyaniline nanocomposite supercapacitor electrodes. Int J Hydrog Energy. 2018;43(40):18617–25.
35. Dogru IB, Durukan MB, Turel O, Unalan HE. Flexible supercapacitor electrodes with vertically aligned carbon nanotubes grown on aluminum foils. Prog Nat Sci. 2016;26(3):232–6.
36. Wang X, Ugur A, Goktas H, Chen N, Wang M, Lachman N, et al. Room temperature resistive volatile organic compound sensing materials based on a hybrid structure of vertically aligned carbon nanotubes and conformal oCVD/iCVD polymer coating. ACS Sens. 2016;1(4):374–83.
37. Azimi S, Farahani A, Sereshti H. Plasma-functionalized highly aligned CNT-based biosensor for point of care determination of glucose in human blood plasma. Electroanalysis. 2020;32(2):394–403.
38. Lin Y, Lu F, Tu Y, Ren Z. Glucose biosensors based on carbon nanotube nanoelectrode ensembles. Nano Lett. 2004;4(2):191–5.
39. Pumera M. The electrochemistry of carbon nanotubes: fundamentals and applications. Chem Eur. 2009;15(20):4970–8.
40. Brownlee BJ, Bahari M, Harb JN, Claussen JC, Iverson BD. Electrochemical glucose sensors enhanced by methyl viologen and vertically aligned carbon nanotube channels. ACS Appl Mater Interfaces. 2018;10(34):28351–60.
41. Raphev VR, Henna TK, Nivitha KP, Mufeedha P, Sabu C, Pramod K. Advanced biomedical applications of carbon nanotube. Mater. Sci. Eng. C. 2019;100:616–30.
42. Yang Y, Li M, Zhu Z. A novel electrochemical sensor based on carbon nanotubes array for selective detection of dopamine or uric acid. Talanta. 2019;201:295–300.
43. Komane PP, Kumar P, Choonara YE, Pillay V. Functionalized, vertically super-aligned multiwalled carbon nanotubes for potential biomedical applications. Int J Mol Sci. 2020;21(7):2276.
44. Varmira K, Mohammadi G, Mahmoudi M, Khodarahmi R, Rashidi K, Hedayati M, et al. Fabrication of a novel enzymatic electrochemical biosensor for determination of tyrosine in some food samples. Talanta. 2018;183:1–10.
45. Jiang H, Wei Z, Cai X, Lai L, Ma J, Haung W. A cathode for Li-ion batteries made of vanadium oxide on vertically aligned carbon nanotube arrays/graphene foam. Chem Eng J. 2019;359:1668–76.
46. Ji D, Liu L, Li S, Chen C, Lu Y, Wu J, et al. Smartphone-based cyclic voltammetry system with graphene modified screen printed electrodes for glucose detection. Biosens Bioelectron. 2017;98:449–56.
47. Feng X, Cheng H, Pan Y, Zheng H. Development of glucose biosensors based on nanostructured graphene-conducting polyaniline composite. Biosens Bioelectron. 2015;70:411–7.
48. Ávila-Orta CA, Cruz-Delgado VJ, Neira-Velázquez MG, Hernández-Hernández E, Méndez-Padilla MG, Medellín-Rodríguez FJ. Surface modification of carbon nanotubes with ethylene glycol plasma. Carbon. 2009;47(8):1916–21.
49. Akhtar MA, Batool R, Hayat A, Han D, Riaz S, Khan SU, et al. Functionalized graphene oxide bridging between enzyme and au-sputtered screen-printed interface for glucose detection. ACS Appl Nano Mater. 2019;2(3):1589–95.
50. Phetsang S, Jakmunee J, Mungkornasawakul P, Laocharoensuk R, Ounnunkad K. Sensitive amperometric biosensors for detection of glucose and cholesterol using a platinum/reduced graphene oxide/poly (3-aminobenzoic acid) film-modified screen-printed carbon electrode. Bioelectrochemistry. 2019;127:125–35.
51. Jose MV, Marx S, Murata H, Koepsel RR, Russell AJ. Direct electron transfers in a mediator-free glucose oxidase-based carbon nanotube-coated biosensor. Carbon. 2012;50(11):4010–20.
52. Soylemez S, Kaya HZ, Adum YA, Toppare L. A multipurpose conjugated polymer: electrochromic device and biosensor construction for glucose detection. Org Electron. 2019;65:327–33.
53. Guan H, Gong D, Song Y, Han B, Zhang N. Biosensor composed of integrated glucose oxidase with liposome microreactors/chitosan nanocomposite for amperometric glucose sensing. Colloids Surf A Physicochem Eng Asp. 2019;574:260–7.
54. Al-Sagur H, Komathi S, Khan MA, Gurek AG, Hassan A. A novel glucose sensor using lutetium phthalocyanine as redox mediator in reduced graphene oxide conducting polymer multifunctional hydrogel. Biosens Bioelectron. 2017;92:638–45.
55. Chen C, Ran R, Yang Z, Lv R, Shen W, Kang F, et al. An efficient flexible electrochemical glucose sensor based on carbon nanotubes/carbonized silk fabrics decorated with Pt microspheres. Sens Actuators B Chem. 2018;256:63–70.
56. Senel M. Simple method for preparing glucose biosensor based on in-situ polypyrrole cross-linked chitosan/glucose oxidase/gold bionanocomposite film. Mater Sci Eng C. 2015;48:287–93.
57. Savk A, Aydin H, Cellat K, Sen F. A novel high performance non-enzymatic electrochemical glucose biosensor based on activated carbon-supported Pt-Ni nanocomposite. J Mol Liq. 2020;300:112355.